Inorg. Chem. **2009**, *48*, 3382−3395

Forum

Magnetic Exchange Coupling in Actinide-Containing Molecules

Jeffrey D. Rinehart, T. David Harris, Stosh A. Kozimor, Bart M. Bartlett, and Jeffrey R. Long*

Department of Chemistry, University of California, Berkeley, California 94720-1460

Received July 12, 2008

Recent progress in the assembly of actinide-containing coordination clusters has generated systems in which the first glimpses of magnetic exchange coupling can be recognized. Such systems are of interest owing to the prospects for involving 5f electrons in stronger magnetic exchange than has been observed for electrons in the more contracted 4f orbitals of the lanthanide elements. Here, we survey the actinide-containing molecules thought to exhibit magnetic exchange interactions, including multiuranium, uranium−lanthanide, uranium−transition metal, and uranium−radical species. Interpretation of the magnetic susceptibility data for compounds of this type is complicated by the combination of spin−orbit coupling and ligand-field effects arising for actinide ions. Nevertheless, for systems where analogues featuring diamagnetic replacement components for the non-actinide spin centers can be synthesized, a data subtraction approach can be utilized to probe the presence of exchange coupling. In addition, methods have been developed for employing the resulting data to estimate lower and upper bounds for the exchange constant. Emphasis is placed on evaluation of the linear clusters (cyclam)M[(μ-Cl)U(Me_2Pz)$_4$]$_2$ (M = Co, Ni, Cu, Zn; cyclam = 1,4,8,11-tetraazacyclotetradecane; Me_2Pz^- = 3,5-dimethylpyrazolate), for which strong ferromagnetic exchange with 15 cm^{-1} ≤ J ≤ 48 cm^{-1} is observed for the Co^{II}-containing species. Owing to the modular synthetic approach employed, this system in particular offers numerous opportunities for adjusting the strength of the magnetic exchange coupling and the total number of unpaired electrons. To this end, the prospects of such modularity are discussed through the lens of several new related clusters. Ultimately, it is hoped that this research will be of utility in the development of electronic structure models that successfully describe the magnetic behavior of actinide compounds and will perhaps even lead to new actinide-based single-molecule magnets.

Introduction

Interest in the magnetic properties of actinide-containing compounds stems from their unique characteristics relative to transition metal- and lanthanide-containing magnetic materials. In many ways, these characteristics can be seen as a blending of the typical magnetic behavior associated with lanthanide compounds, such as spin−orbit coupling and relativistic effects, with that observed in transition metal compounds, such as strong magnetic superexchange. While the magnetic properties of actinide-containing complexes are of interest on a fundamental level, they can also potentially be exploited in producing discrete molecules that exhibit slow magnetic relaxation.[1] Such molecules are known as single-molecule magnets (SMMs), and their unusual behavior arises from the influence of a negative axial magnetic anisotropy, D, on a high-spin ground state, S. The resulting relaxation barrier of $U = S^2|D|$ for integer S values [or $U = (S^2 - {}^1/_4)|D|$ for half-integer S values] is, at most, 60 cm^{-1} for known transition metal clusters.[1d] The possibility of increasing this barrier height, and perhaps opening the way for potential applications,[1c,2] provides impetus for the development of new approaches to generating SMMs.

Transition metals have served extremely well for generating discrete clusters, wherein strong magnetic coupling

* To whom correspondence should be addressed. E-mail: jrlong@berkeley.edu.

(1) (a) Sessoli, R.; Tsai, H. L.; Schake, A. R.; Wang, S.; Vincent, J. B.; Folting, K.; Gatteschi, D.; Christou, G.; Hendrickson, D. N. *J. Am. Chem. Soc.* **1993**, *115*, 1804. (b) Sessoli, R.; Gatteschi, D.; Caneschi, A.; Novak, M. A. *Nature* **1993**, *365*, 141. (c) Gatteschi, D.; Sessoli, R.; Villain, J. *Molecular Nanomagnets*; Oxford University Press: New York, 2006 and references cited therein. (d) Milios, C. J.; Vinslava, A.; Wernsdorfer, W.; Moggach, S.; Parsons, S.; Perlepes, S. P.; Christou, G.; Brechin, E. K. *J. Am. Chem. Soc.* **2007**, *129*, 2754.

10.1021/ic801303w CCC: $40.75
Published on Web 04/13/2009

between many metal centers gives rise to concerted behavior with a large total spin quantum number, S.[3] However, owing to their large single-ion anisotropies, some of the systems exhibiting the largest relaxation barriers instead contain lanthanide ions.[4] Indeed, the anisotropy associated with lanthanide ions such as Tb^{3+} and Dy^{3+} has led to manifestations of slow magnetic relaxation, even in molecules containing just one metal center.[5] These examples demonstrate the great promise of f elements in the future of SMM chemistry, especially if their single-ion properties could be incorporated into high-nuclearity clusters where the spin and axial anisotropy of many metals could contribute to the energy barrier to spin inversion. However, it is difficult to envision high-nuclearity lanthanide clusters with concerted spin behavior because the 4f valence orbitals typically lack the radial extension and energetic proximity required for significant overlap with bridging ligand orbitals.[6] This results in small covalent interactions and weak pathways for magnetic superexchange through diamagnetic bridging ligands. In contrast, the greater radial extension of the 5f valence orbitals of actinides can potentially provide increased overlap with bridging ligand orbitals, thereby enhancing the concerted magnetic behavior between bridged metal centers within a single cluster unit.[6a,7]

In this Forum, we survey recent developments in the synthesis and characterization of molecular systems in which actinide ions potentially engage in magnetic exchange interactions. Thus far, efforts have focused exclusively on species incorporating uranium because this actinide element offers minimal radioactivity (in depleted form) with accessible oxidation states allowing for zero, one, two, or three unpaired electrons. Researchers have confronted the intricacies of the magnetic exchange in a number of interesting ways, often with the goal of identifying and, to the extent possible, quantifying ferro- or antiferromagnetic exchange coupling. Understanding these exchange interactions not only is essential to the development of models for the basic electronic structure of the 5f elements but also may represent the key to producing the first actinide-based SMMs.

Challenges in Interpreting the Magnetic Behavior of Actinide Compounds

Despite a growing number of varied synthetic systems incorporating paramagnetic uranium centers, unraveling actinide magnetic behavior remains a challenge because of the lack of a theoretical foundation for accurately modeling the complex interactions that govern actinide magnetic susceptibility. In the molecular chemistry of first-row transition metal ions, it is usually possible to treat the magnetic susceptibility as being due to the unpaired spins, with minimal effects from the orbital components owing to an orbital angular momentum that is largely quenched by the ligand field. The "spin-only" approximation, which works reasonably well for most first-row transition metal species, loses its validity for a number of molecular systems of interest for magnetism, including those containing actinide ions.[8] For example, a U^{IV} center possesses two unpaired 5f electrons, leading to a ^3H ($S = 1$, $L = 5$) ground state. Spin−orbit coupling produces an energy splitting based on the total angular momentum, J, where $|S - L| \leq J \leq L + S$. For the U^{IV} ion, which has a less than half-filled 5f shell, this leads to a $^3H_4$ designation for the spin−orbit-coupled ground state. Depending on the degree of spin−orbit coupling, mixing with excited-state Russell−Saunders terms of the same J value can occur. Recent calculations on the U^{IV} ion suggest that the $^3H_4$ ground state can have significant

(2) (a) Garanin, D. A.; Chudnovsky, E. M. *Phys. Rev. B* **1997**, *56*, 11102. (b) Leuenberger, M. N.; Loss, D. *Nature* **2001**, *410*, 789. (c) Heersche, H. B.; de Groot, Z.; Folk, J. A.; van der Zant, H. S. J.; Romeike, C.; Wegewijs, M. R.; Zobbi, L.; Barreca, D.; Tondello, E.; Cornia, A. *Phys. Rev. Lett.* **2006**, *96*, 206801. (d) Jo, M.-H.; Grose, J. E.; Liang, W.; Baheti, K.; Deshmukh, M. M.; Sokol, J. J.; Rumberger, E. M.; Hendrickson, D. N.; Long, J. R.; Park, H.; Ralph, D. C. *Nano Lett.* **2006**, *6*, 2014.

(3) (a) Powell, A. K.; Heath, S. L.; Gatteschi, D.; Pardi, L.; Sessoli, R.; Spina, G.; Del Giallo, F.; Pieralli, F. *J. Am. Chem. Soc.* **1995**, *117*, 2491. (b) Zhong, Z. J.; Seino, H.; Mizobe, Y.; Hidai, M.; Fujishima, A.; Ohkoshi, S.; Hashimoto, K. *J. Am. Chem. Soc.* **2000**, *122*, 2952. (c) Murugesu, M.; Habrych, M.; Wernsdorfer, W.; Abboud, K. A.; Christou, G. *J. Am. Chem. Soc.* **2004**, *126*, 4766. (d) Ako, A. M.; Hewitt, I. J.; Mereacre, V.; Clérac, R.; Wernsdorfer, W.; Anson, C. E.; Powell, A. K. *Angew. Chem., Int. Ed.* **2006**, *45*, 4926.

(4) (a) Osa, S.; Kido, T.; Matsumoto, N.; Re, N.; Pochaba, A.; Mrozinski, J. *J. Am. Chem. Soc.* **2004**, *126*, 420. (b) Mishra, A.; Wernsdorfer, W.; Abboud, K. A.; Christou, G. *J. Am. Chem. Soc.* **2004**, *126*, 15648. (c) Zaleski, C. M.; Depperman, E. C.; Kampf, J. W.; Kirk, M. L.; Pecoraro, V. L. *Angew. Chem., Int. Ed.* **2004**, *43*, 3912. (d) Mishra, A.; Wernsdorfer, W.; Parsons, S.; Christou, G.; Brechin, E. K. *Chem. Commun.* **2005**, 2086. (e) Mori, F.; Nyui, T.; Ishida, T.; Nogami, T.; Choi, K.-y.; Nojiri, H. *J. Am. Chem. Soc.* **2006**, *128*, 1440. (f) Tang, J.; Hewitt, I.; Madhu, N. T.; Chastanet, G.; Wernsdorfer, W.; Anson, C. E.; Benelli, C.; Sessoli, R.; Powell, A. K. *Angew. Chem., Int. Ed.* **2006**, *45*, 1729. (g) Ferbinteanu, M.; Kajiwara, T.; Choi, K.-y.; Nojiri, H.; Nakamoto, A.; Kojima, N.; Cimpoesu, F.; Fujimura, Y.; Takaishi, S.; Yamashita, M. *J. Am. Chem. Soc.* **2006**, *128*, 9008. (h) Tangoulis, V.; Figuerola, A. *Chem. Phys.* **2007**, *340*, 293. (i) Chandrasekhar, V.; Pandian, B. M.; Boomishankar, R.; Steiner, A.; Vittal, J. J.; Houri, A.; Clérac, R. *Inorg. Chem.* **2008**, *47*, 4918. (j) Lin, P.-H.; Burchell, T. J.; Clérac, R.; Murugesu, M. *Angew. Chem., Int. Ed.* **2008**, *47*, 8848.

(5) (a) Ishikawa, N.; Sugita, M.; Ishikawa, T.; Koshihara, S.; Kaizu, Y. *J. Am. Chem. Soc.* **2003**, *125*, 8694. (b) Ishikawa, N.; Sugita, M.; Ishikawa, T.; Koshihara, S.; Kaizu, Y. *J. Phys. Chem. B* **2004**, *108*, 11265. (c) Ishikawa, N.; Sugita, M.; Wernsdorfer, W. *Angew. Chem., Int. Ed.* **2005**, *44*, 2931. (d) Takamatsu, S.; Ishikawa, T.; Koshihara, S.-y.; Ishikawa, N. *Inorg. Chem.* **2007**, *46*, 7250. (e) AlDamen, M. A.; Clemente-Juan, J. M.; Coronado, E.; Martí-Gastaldo, C.; Gaita-Ariño, A. *J. Am. Chem. Soc.* **2008**, *130*, 8874.

(6) (a) Crosswhite, H. M.; Crosswhite, H.; Carnall, W. T.; Paszek, A. P. *J. Chem. Phys.* **1980**, *72*, 5103. (b) Costes, J.-P.; Dahan, F.; Dupuis, A.; Laurent, J.-P. *Chem.—Eur. J.* **1998**, *4*, 1616. (c) Kahn, M. L.; Mathonière, C.; Kahn, O. *Inorg. Chem.* **1999**, *38*, 3692. (d) Benelli, C.; Gatteschi, D. *Chem. Rev.* **2002**, *102*, 2369.

(7) Gaunt, A. J.; Reilly, S. D.; Enriquez, A. E.; Scott, B. L.; Ibers, J. A.; Sekar, P.; Ingram, K. I. M.; Kaltsoyannis, N.; Neu, M. P. *Inorg. Chem.* **2008**, *47*, 29.

(8) The discussion of the electronic structure of actinides presented here is meant to give an overview of the complexity of such systems and is by no means comprehensive. For a thorough theoretical analysis, the reader is referred to the following: (a) Wybourne, B. G. *Spectroscopic Properties of Rare Earths*; Wiley: New York, 1965. (b) Siddall, T. H. *Theory and Applications of Molecular Paramagnetism*; Wiley: New York, 1976. (c) Kanellakopulos, B. In *Organometallics of the f-Elements*; Marks, T. J., Fischer, R. D., Eds.; NATO Advanced Study Institutes Series; D. Reidel: Dordrecht, The Netherlands, 1978. (d) Orchard, A. F. *Magnetochemistry*; Oxford University Press Inc.: New York, 2003. (e) Edelstein, N. M.; Lander, G. H. In *The Chemistry of the Actinide and Transactinide Elements*, 3rd ed.; Morss, L. R., Edelstein, N. M., Fuger, J., Eds.; Springer: Dordrecht, The Netherlands, 2006; Vol. *4*, p 2225.

$^1G_4$ character (9% in the case studied).[9] This mixing of excited-state Russell−Saunders terms into the ground state invalidates *S* and *L* as individual quantum numbers and can also restore the orbital angular momentum by mixing other f orbitals into the ground-state wave function.

The above methodology for describing the electronic structure of the U^{IV} ion, wherein spin−spin repulsions are considered, followed by coupling of the spin and orbital angular momenta, and then allowing for the mixing of *J* states is known as an intermediate coupling scheme. While we choose to start from the more familiar Russell−Saunders coupling scheme, the electronic structure of actinides could be described equally well by first coupling the individual spin and orbital angular momenta of each electron (*j*−*j* coupling scheme), then applying the interelectronic repulsions, and finally allowing for mixing of the *J* states. Because neither the Russell−Saunders method nor the *j*−*j* coupling method alone accurately describes the electronic structure of actinides, this sort of intermediate coupling scheme is necessary.

The discussion thus far has neglected the effects of the ligand field. While the electronic structure perturbations of the ligand field are not nearly as noticeable for actinides as for transition metals, the radial extension of the 5f orbitals does allow for metal−ligand interaction. Therefore, it is necessary to consider the ligand-field effects as a perturbation on the spin−orbit-coupled ground-state configuration. This perturbation removes the $(2J + 1)$-fold degeneracy of the ground state. The resulting sublevel splitting is often referred to as the Stark splitting, and the states themselves are referred to as Stark sublevels. The degeneracy of these sublevels is determined by symmetry; however, in accordance with Kramers rule, the degeneracy of odd electron systems cannot be completely lifted regardless of the ligand field. The ordering of these sublevels is subtly affected by the orientation and strength of the ligand field and cannot be predicted in a straightforward manner. The irregularity of the Stark splitting is further complicated by mixing between the Stark sublevels of the spin−orbit-coupled ground state and the excited states.

The complexity of the electronic structure for a single actinide ion is both exciting and frustrating in terms of its effects on the magnetic properties of a molecular cluster. Of particular note is the anisotropy to the orientation of the angular momentum created by the ligand-field Stark splitting. When magnetically coupled to the spins of other metals, this single-ion anisotropy could give rise to a large energy barrier between orientations of the ground-state spin of the molecule, thereby possibly leading to SMMs with a high blocking temperature. The realization of such phenomena may greatly depend on the ability to characterize the magnetic exchange coupling between ligand-bridged metal centers. However, in order to verify such an interaction between metal centers, it is necessary to investigate the variable-temperature magnetic susceptibility for evidence of magnetic exchange coupling, a task complicated by the intricacy of the actinide-ion electronic structure. The electronic complexity leads to a strong variation in the thermal population of the many states energetically comparable to the ground state. This effect becomes evident as the higher-energy Stark sublevels depopulate as the temperature is lowered. Depopulation of these sublevels leads to a concomitant decrease in the magnitude of the total angular momentum vector. Two important consequences arise from this phenomenon. First, the decrease in the angular momentum manifests itself as a decrease in the magnetic susceptibility, which can obscure other simultaneous effects, such as magnetic exchange coupling between bridged metal centers. Additionally, if such an exchange coupling between the actinide ion and other metals in the cluster does exist, its magnitude will decrease, and in the case of low-symmetry non-Kramers systems, eventually disappear at low temperature because there is less angular momentum to which the spin of the non-actinide center can couple. Dealing with these single-ion effects, which both obscure and interfere with the effects of magnetic coupling between metal centers, is of preeminent importance to the progression of the field of actinide molecular magnetism.

Attempts to model the ligand field and extract exchange coupling data by fitting to an appropriate Hamiltonian have been employed for both lanthanide and actinide systems, which have a single, well-isolated Stark sublevel ground state. However, complications arise when modeling the temperature-dependent magnetic effects due to subtle shifts in the Stark sublevels.[10] Attempting to model many variables can easily lead to overparameterization, so several groups have circumvented these issues by attempting to synthesize a compound isostructural to the molecule of interest, wherein the non-f-element paramagnetic center has been replaced by a diamagnetic one. Then, subtraction of the two data sets is performed to simulate removal of the orbital and ligand-field effects of the f-element ion, thereby exposing any magnetic exchange coupling interactions. Although extremely dependent on small changes in the ligand field, such a model has been applied successfully to numerous lanthanide-containing systems.[11] This subtraction method is also currently the most widely employed method for interpreting uranium magnetism and will be discussed in detail below.

Survey of Molecules Potentially Exhibiting Magnetic Exchange

A Diuranium Complex. The first observation of magnetic exchange coupling in an actinide-containing molecule was reported nearly 20 years ago for the binuclear, 1,4-diimidobenzene-bridged complex $[(MeC_5H_4)_3U]_2(\mu\text{-}1,4\text{-}N_2C_6H_4)$.[12] The presence of coupling between the two U^V centers within this molecule became evident upon a comparison of its variable-temperature magnetic susceptibility to that of struc-

(9) Danilo, C.; Vallet, V.; Flament, J.-P.; Wahlgren, U. *J. Chem. Phys.* **2008**, *128*, 154310.

(10) Kahn, M. L.; Rafik, B.; Porcher, P.; Kahn, O.; Sutter, J.-P. *Chem.—Eur. J.* **2002**, *8*, 525.

(11) Sutter, J.-P.; Kahn, M. L. In *Magnetism: Molecules to Materials V*; Miller, J. S., Drillon, M., Eds.; Wiley-VHC: Weinheim, Germany, 2001; pp 161−187 and references cited therein.

(12) Rosen, R. K.; Andersen, R. A.; Edelstein, N. M. *J. Am. Chem. Soc.* **1990**, *112*, 4588.

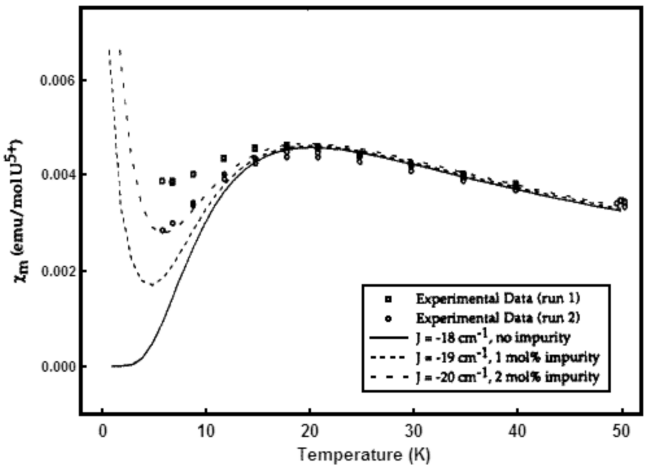

Figure 1. Experimental (symbols) versus calculated (lines) molar magnetic susceptibility for $[(MeC_5H_4)_3U]_2(\mu\text{-}1,4\text{-}N_2C_6H_4)$. Each calculated curve is modeled with a different amount of the paramagnetic impurity, $(MeC_5H_4)_3U(THF)$. Taken from ref 12.

turally similar compounds. The geometric isomer $[(MeC_5H_4)_3U]_2(\mu\text{-}1,3\text{-}N_2C_6H_4)$, for instance, displays essentially constant magnetic susceptibility (χ_M) with decreasing temperature from 300 K down to ca. 150 K, at which point it begins to rise monotonically as the temperature is decreased to 5 K. This behavior, typical of an isolated $5f^1$ center, is essentially the sum of that observed for two $(MeC_5H_4)_3U(NPh)$ complexes and indicates the lack of any magnetic exchange between the two U^V centers.[12,13] In contrast, the magnetic susceptibility data obtained for $[(MeC_5H_4)_3U]_2(\mu\text{-}1,4\text{-}N_2C_6H_4)$ display similar behavior down to ca. 75 K but then exhibit a downturn at lower temperatures, indicative of antiferromagnetic coupling (see Figure 1).

In an attempt to obtain a quantitative determination of the coupling in $[(MeC_5H_4)_3U]_2(\mu\text{-}1,4\text{-}N_2C_6H_4)$, the experimental χ_M vs T data were compared to calculated susceptibilities. The magnetic interaction between the U^V centers was modeled by employing the following Ising Hamiltonian for an isolated dinuclear complex:

$$H = -2J(\hat{S}_{z1} \cdot \hat{S}_{z2}) + g_{||}\mu_B \hat{H}_z \cdot (\hat{S}_{z1} + \hat{S}_{z2}) \qquad (1)$$

where $\hat{S}_{zn}$ is the effective spin operator for each $S = {}^1/_2$ U^V ion (the z direction is defined as along the U···U axis), J is the exchange constant, $g_{||}$ is the Landé g factor, μ_B is the Bohr magneton, and $\hat{H}_z$ is the magnetic field vector. Note that this Hamiltonian does not account for deviations in the magnetic susceptibility resulting from depopulation of the uranium Stark sublevels with decreasing temperature but rather it assumes such deviations arise solely from exchange between two $S = {}^1/_2$ ions. This assumption was made based on an analysis of the electron paramagnetic resonance (EPR) spectrum, which suggested that only the lowest Stark sublevel is populated at low temperature. The $J = {}^5/_2$ ground state for a U^V center is split by the ligand field into three Stark sublevels, two corresponding to $\mu = \pm{}^1/_2$ and one corresponding to $\mu = \pm{}^3/_2$, where μ is the crystal quantum number.[8a] Considering EPR selection rules, a spectrum is expected for a sublevel with crystal quantum number $\mu = \pm{}^1/_2$, while no spectrum is expected for a sublevel with crystal quantum number $\mu = \pm{}^3/_2$. The uncoupled dinuclear complex, $[(MeC_5H_4)_3U]_2(\mu\text{-}1,3\text{-}N_2C_6H_4)$, gave no EPR spectrum at 4 K, suggesting population of only the lowest-energy Stark sublevel, $\mu = \pm{}^3/_2$. Thus, the drop in the magnetic susceptibility of $[(MeC_5H_4)_3U]_2(\mu\text{-}1,4\text{-}N_2C_6H_4)$, at least at such very low temperatures, can be attributed to magnetic exchange rather than the usual effects of the Stark sublevel depopulation. Figure 1 shows the resulting calculated and experimental susceptibility data. The differences between the two experimental data sets were attributed to sample impurity and, as such, the calculated data were modeled with varying amounts of paramagnetic impurity. On the basis of these parameters, the best fit was obtained with an exchange constant of $J = -19$ cm^{-1} and an estimated paramagnetic impurity of 1 mol %.

Other Multiuranium Systems. Although our focus is on actinide-containing molecules for which the occurrence of magnetic coupling has been directly probed, there are a number of intriguing multiuranium systems wherein magnetic exchange is likely but has not been rigorously investigated. For example, attempts to produce clusters that might feature uranium−uranium bonds led to a number of simple diuranium alkoxides, including $[U_2(O_2CMe_3)_9]^{0/1-}$,[14] and the chloro-bridged species $[(C_6Me_6)_2U_2Cl_7]^-$.[15] On the basis of the assumption that nitrogenous ligands promote bridging in actinides,[16] a number of di-, tri-, and tetranuclear uranium amide species were synthesized, including the dinuclear complex $[U(\eta\text{-}C_8H_8)]_2[\mu\text{-}\eta^4\text{:}\eta^4\text{-}HN(CH_2)_3N(CH_2)_2N(CH_2)_3\text{-}NH]$, which contains the shortest U···U separation yet observed in a molecule.[17] Diuranium systems featuring an arene bridge, such as $[(Mes(^tBu)N)_2U]_2(\mu\text{-}\eta^6\text{:}\eta^6\text{-}C_7H_8)$ and $[(Cp^*)_2U]_2(\mu\text{-}\eta^6\text{:}\eta^6\text{-}C_6H_6)$,[18] and the pyrazolate-bridged dimer $[U(Me_2Pz)_4]_2$ (Me_2Pz^- = 3,5-dimethylpyrazolate),[19] also present the strong possibility of magnetic exchange coupling.

While the foregoing examples constitute only a fraction of the molecular uranium clusters that might exhibit magnetic exchange coupling, they do serve to give an idea of how much synthetic work has already been accomplished in the area. In addition, symmetric dinuclear complexes such as these would serve well in testing general electronic structure models attempting to account for the influence of exchange coupling on the magnetic behavior of actinide ions. Given

(13) Graves, C. R.; Yang, P.; Kozimor, S. A.; Vaughn, A. E.; Clark, D. L.; Conradson, S. D.; Schelter, E. J.; Scott, B. L.; Thompson, J. D.; Hay, P. J.; Morris, D. E.; Kiplinger, J. L. *J. Am. Chem. Soc.* **2008**, *130*, 5272.

(14) Cotton, F. A.; Marler, D. O.; Schwotzer, W. *Inorg. Chem.* **1984**, *23*, 4211.

(15) Cotton, F. A.; Schwotzer, W. *Organometallics* **1985**, *4*, 942.

(16) Reynolds, J. G.; Zalkin, A.; Templeton, D. H.; Edelstein, N. M.; Tempelton, L. K. *Inorg. Chem.* **1976**, *15*, 2498.

(17) (a) Berthet, J. C.; Ephritikhine, M. *Coord. Chem. Rev.* **1998**, *178*, 83. (b) Borgne, T. L.; Lance, M.; Nierlich, M.; Ephritikhine, M. *J. Organomet. Chem.* **2000**, *598*, 313.

(18) (a) Diaconescu, P. L.; Arnold, P. L.; Baker, T. A.; Mindiola, D. J.; Cummins, C. C. *J. Am. Chem. Soc.* **2000**, *122*, 6108. (b) Diaconescu, P. L.; Cummins, C. C. *J. Am. Chem. Soc.* **2002**, *124*, 7660. (c) Evans, W. J.; Kozimor, S. A.; Ziller, J. W.; Kaltzoyannis, N. *J. Am. Chem. Soc.* **2004**, *126*, 14533.

(19) Kozimor, S. A.; Bartlett, B. M.; Rinehart, J. D.; Long, J. R. *J. Am. Chem. Soc.* **2007**, *129*, 10672.

the current lack of reliable models, a significant step toward probing the presence of exchange coupling in such species would be the development of synthetic methods for preparing mixed-actinide analogues, wherein one of the two actinide centers is rendered diamagnetic. Here, the replacement of one of the U^{IV} centers with a Th^{IV} center, or one of the U^{III} centers with an Ac^{III} center,[20] would enable a subtraction approach of the type elaborated below to be applied in providing a qualitative assessment of the exchange coupling.

Another type of uranium-containing molecule that offers promise in the area of molecular magnetism is the high-nuclearity uranium oxo cluster. While most oxo-bridged uranium complexes are di- or trinuclear species,[21] it was recently shown that hydrolysis of $UI_3(THF)_4$ in the presence of water and other ligands can result in higher-nuclearity clusters.[22] The largest of these is the discrete dodecanuclear species $U_{12}(\mu_3\text{-}O)_{12}(\mu_3\text{-}OH)_8I_2(\mu_2\text{-}O_3SCF_3)_{16}(CH_3CN)_8$, which contains a double-decker square-antiprism $U_{12}O_{12}(OH)_8$ core.[22d] This type of cluster, while well beyond the scope of current techniques for analyzing magnetic exchange coupling, may offer prospects for observation of the SMM behavior in uranium systems. Indeed, such clusters could potentially combine the desirable properties of large spin and single-ion anisotropy with the high coupling strength of the oxo bridge.

A Uranium−Lanthanide System. Recently, evidence of exchange coupling was reported for the bent trinuclear 4f−5f cluster $Cp^*_2U[(NC(CH_2C_6H_5)tpy)YbCp^*_2]_2$ (UYb_2; tpy = terpyridyl).[23] The structure of this species features a central $[Cp^*_2U^{IV}]^{2+}$ unit connected through $NC(CH_2C_6H_5)tpy$ bridges to two $[Cp^*_2Yb]^{x+}$ ($x = 0$ or 1) moieties, as shown in Figure 2. The cyclic voltammetry and electronic absorption spectra of the UYb_2 cluster suggest the presence of both $Cp^*_2Yb^{II}tpy$ and $Cp^*_2Yb^{III}tpy^{\bullet}$ species at room temperature.[24] The variable-temperature magnetic susceptibility data obtained for the cluster are plotted in Figure 3. Here, $\chi_M T$ follows a gradual downward trend from 350 K to ca. 25 K, followed by a precipitous drop at lower temperatures, which can be understood largely in terms of the orbital angular momentum quenching discussed above for $5f^1$ systems. However, the gradual decline in $\chi_M T$ from its room temperature value is characteristic of multielectron f-element-containing complexes and is generally attributed to thermal depopulation of the Stark sublevels.[8] However, the behavior observed here is further complicated by the presence of both diamagnetic Yb^{II} and paramagnetic Yb^{III} ions, in addition to an unpaired electron residing on the terpyridine fragment.

In an attempt to deconvolute the magnetic data and extract information regarding potential exchange interactions between the U^{IV} and Yb^{III} centers, a stepwise series of subtractions was performed on the UYb_2 data. First, $\chi_M T$ data collected for the precursor complex $Cp^*_2U(NC(CH_2C_6H_5)tpy)_2$ were subtracted from the UYb_2 data to remove any orbital contribution from the U^{IV} ion to the overall magnetism. Then, to eliminate the magnetic contribu-

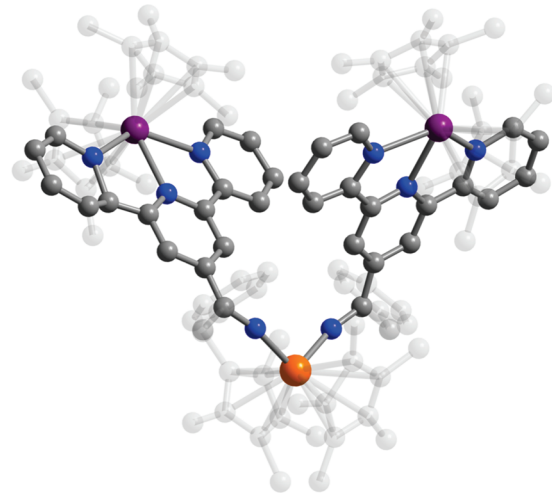

Figure 2. Structure of $Cp^*_2U[(NC(CH_2C_6H_5)tpy)YbCp^*_2]_2$.[23] Orange, purple, blue, and gray spheres represent U, Yb, N, and C atoms, respectively. H atoms are omitted for clarity. The Cp* ligands and benzyl groups are drawn transparently for better visualization of the core structure.

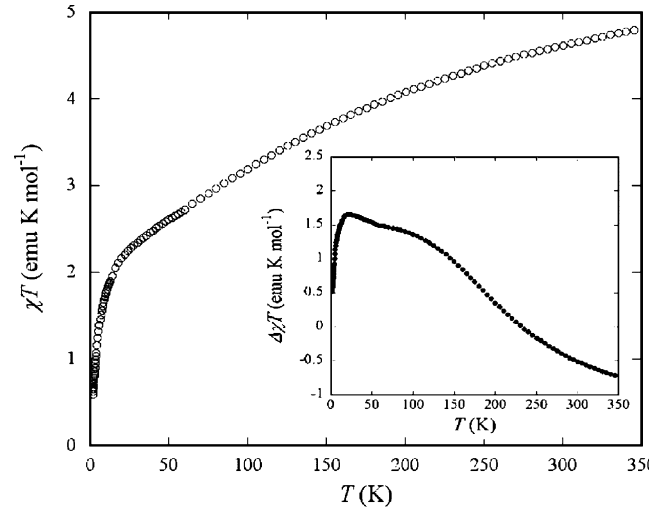

Figure 3. Variable-temperature magnetic susceptibility data for $Cp^*_2U[(NC(CH_2C_6H_5)tpy)YbCp^*_2]_2$. Inset: Variable-temperature magnetic susceptibility data obtained upon subtraction of data for $Cp^*_2U(NC(CH_2C_6H_5)tpy)_2$ and $Cp^*_2Th[(NC(CH_2C_6H_5)tpy)YbCp^*_2]_2$ from the UYb_2 data. Taken from ref 23.

(20) Note, however, that accomplishing this substitution would involve very serious difficulties stemming from the extreme radioactivity of actinium isotopes.

(21) (a) Berthet, J.-C.; Le Maréchal, J.-F.; Nierlich, M.; Lance, M.; Vigner, J.; Ephritikhine, M. *J. Organomet. Chem.* **1991**, *408*, 335. (b) Lukens, W. W., Jr.; Allen, P. G.; Bucher, J. J.; Edelstein, N. M.; Hudson, E. A.; Shuh, D. K.; Reich, T.; Andersen, R. A. *Organometallics* **1999**, *18*, 1253. (c) Korobkov, I.; Gambarotta, S.; Yap, G. P. A. *Organometallics.* **2001**, *20*, 2552. (d) Castro-Rodriguez, I.; Olsen, K.; Gantzel, P.; Meyer, K. *Chem. Commun.* **2002**, 2764. (e) Karmazin, L.; Mazzanti, M.; Pécaut, J. *Inorg. Chem.* **2003**, *42*, 5900. (f) Enriquez, A. E.; Scott, B. L.; Neu, M. P. *Inorg. Chem.* **2005**, *44*, 7403. (g) Salmon, L.; Thuèry, P.; Asfari, Z.; Ephritikhine, M. *Dalton Trans.* **2006**, *24*, 3006. (h) Christopher, P.; Larch, F.; Cloke, G. N.; Hitchcock, P. B. *Chem. Commun.* **2008**, 82.

(22) (a) Mokry, L. M.; Dean, N. S.; Carrano, C. J. *Angew. Chem., Int. Ed.* **1996**, *35*, 1497. (b) Duval, P. B.; Burns, C. J.; Clark, D. L.; Morris, D. E.; Scott, B. L.; Thompson, J. D.; Werkema, E. L.; Jia, L.; Andersen, R. A. *Angew. Chem., Int. Ed.* **2001**, *40*, 3357. (c) Berthet, J.-C.; Thuery, P.; Ephritikhine, M. *Chem. Commun.* **2005**, 3415. (d) Nocton, G.; Burdet, F.; Pécaut, J.; Mazzanti, M. *Angew. Chem., Int. Ed.* **2007**, *46*, 7574.

(23) Schelter, E. J.; Veauthier, J. M.; Thompson, J. D.; Scott, B. L.; John, K. D.; Morris, D. E.; Kiplinger, J. L. *J. Am. Chem. Soc.* **2006**, *128*, 2198.

(24) Veauthier, J. M.; Schelter, E. J.; Kuehl, C. J.; Clark, A. E.; Scott, B. L.; Morris, D. E.; Martin, R. L.; Thompson, J. D.; Kiplinger, J. L.; John, K. D. *Inorg. Chem.* **2005**, *44*, 5911.

tion from Yb^{III}, $\chi_M T$ data collected for $Cp^*_2Th[(NC(CH_2C_6H_5)tpy)YbCp^*_2]_2$ ($ThYb_2$) were subtracted. The result of these subtractions, shown as $\Delta\chi_M T$ in the inset of Figure 3, is a data set that follows a monotonic increase with decreasing temperature from 350 K to ca. 15 K and then drops precipitously at lower temperatures. The rise in $\Delta\chi_M T$ is interpreted as evidence of exchange coupling within the cluster, although the specific nature of the coupling is unclear because the U^{IV} and Yb^{III} ions and the terpyridine radical represent three distinct paramagnetic centers. The curvature of the data above 60 K is attributed to electronic differences between the UYb_2 and $ThYb_2$ clusters, as evidenced in cyclic voltammetry, where the redox peaks for the two clusters are shifted relative to one another. Furthermore, the authors note that the negative values for $\Delta\chi_M T$ represent an overcorrection during the subtraction process. Thus, while qualitative interpretation of $\Delta\chi_M T$ vs T suggests the presence of magnetic coupling, the complexity of this system may prohibit a quantitative analysis.

The magnetic properties of an analogous trinuclear species, $Cp^*_6U_3(NC(CH_2C_6H_5)tpy)_2$, in which U^{III} replaces both of the Yb centers, exhibit a similar trend where $\chi_M T$ decreases with decreasing temperature.[25] However, the complications encountered in the data analysis of the UYb_2 species, along with the lack of diamagnetic analogues to the $U^{IV}U^{III}_2$ cluster, have thus far made it impossible to deconvolute the many factors contributing to the magnetic susceptibility and isolate evidence of magnetic exchange coupling.

Uranium−Transition Metal Systems. To date, the most comprehensively studied class of actinide-containing molecules exhibiting magnetic exchange interactions is a series of trinuclear uranium−transition metal assemblies synthesized by Ephritikhine and coworkers. These clusters have the form $UL^i_2M_2(py)_n$ (M = Cu, Zn; py = pyridine), where L^i is one of a series of nine Schiff-base bridging ligands, each with a modified diimino hydrocarbon backbone (see Figure 4).[26] The structure of each cluster consists of a central U^{IV} ion coordinated linearly to two M^{II} ions through orthogonal $(L^i)^{4-}$ bridges, as represented in Figure 5. The U^{IV} center resides in a dodecahedral coordination environment, encapsulated by eight O donor atoms. Each M^{II} center is coordinated to two N atoms and two O atoms of the Schiff base in a distorted square-planar geometry and is bound by zero, one, or two pyridine molecules, depending on the bridging ligand. Importantly, the coordination environment around the U^{IV} center remains invariant with changes in the bridging ligand and number of transition metal-coordinated pyridine molecules, suggesting that differences in the magnetic behavior across the series are not due to alterations in the ligand field of the uranium ion.

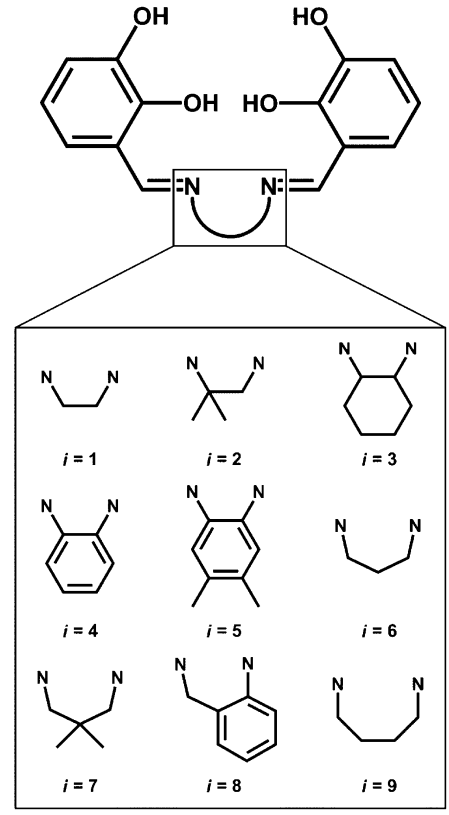

Figure 4. Schematic representation of the ligand precursors H_4L^i. Note the two-carbon backbone for $i = 1-5$, three-carbon backbone for $i = 6-8$, and four-carbon backbone for $i = 9$.

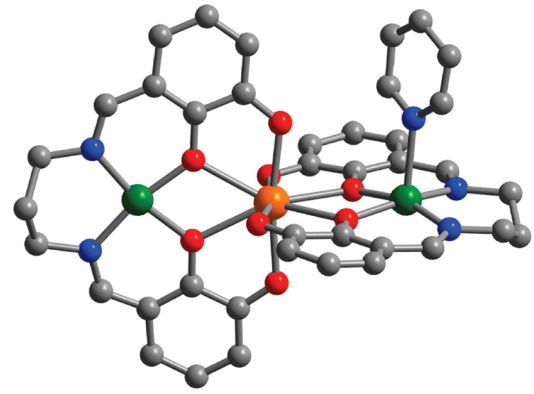

Figure 5. Structure of $UL^6_2Cu_2(py)$. Orange, green, red, blue, and gray spheres represent U, Cu, O, N, and C atoms, respectively. H atoms are omitted for clarity.

The isolation of isostructural copper and zinc analogues of the $UL^i_2M_2(py)_n$ clusters enabled the use of a subtraction method similar to the one described above, thereby providing a route through which to investigate the magnetic interaction between the U^{IV} and Cu^{II} ions without contamination by single-ion effects of U^{IV}. Variable-temperature magnetic susceptibility data for $UL^7_2M_2(py)$ (M = Cu, Zn) are shown at the top of Figure 6. For the UZn_2 cluster, $\chi_M T$ remains essentially constant at 0.8 $cm^3 \cdot K/mol$ as the temperature is lowered from 300 to 100 K and then drops precipitously at lower temperatures, tending toward zero at 2 K. This drop, typical of U^{IV} complexes with a $5f^2$ valence electron configuration, can be attributed to the depopulation of the Stark sublevels and subsequent quenching of the total angular

(25) Schelter, E. J.; Wu, R.; Scott, B. L.; Thompson, J. D.; Morris, D. E.; Kiplinger, J. L. *Angew. Chem., Int. Ed.* **2008**, *47*, 2993.

(26) (a) Le Borgne, T.; Rivière, E.; Marrot, J.; Girerd, J.-J.; Ephritikhine, M. *Angew. Chem., Int. Ed.* **2000**, *39*, 1647. (b) Le Borgne, T.; Rivière, E.; Marrot, J.; Thuéry, P.; Girerd, J.-J.; Ephritikhine, M. *Chem.—Eur. J.* **2002**, *8*, 774. (c) Salmon, L.; Thuéry, P.; Rivière, E.; Girerd, J.-J.; Ephritikhine, M. *Chem. Commun.* **2003**, 762. (d) Salmon, L.; Thuéry, P.; Rivière, E.; Girerd, J.-J.; Ephritikhine, M. *Dalton Trans.* **2003**, 2872. (e) Salmon, L.; Thuéry, P.; Rivière, E.; Ephritikhine, M. *Inorg. Chem.* **2006**, *45*, 83.

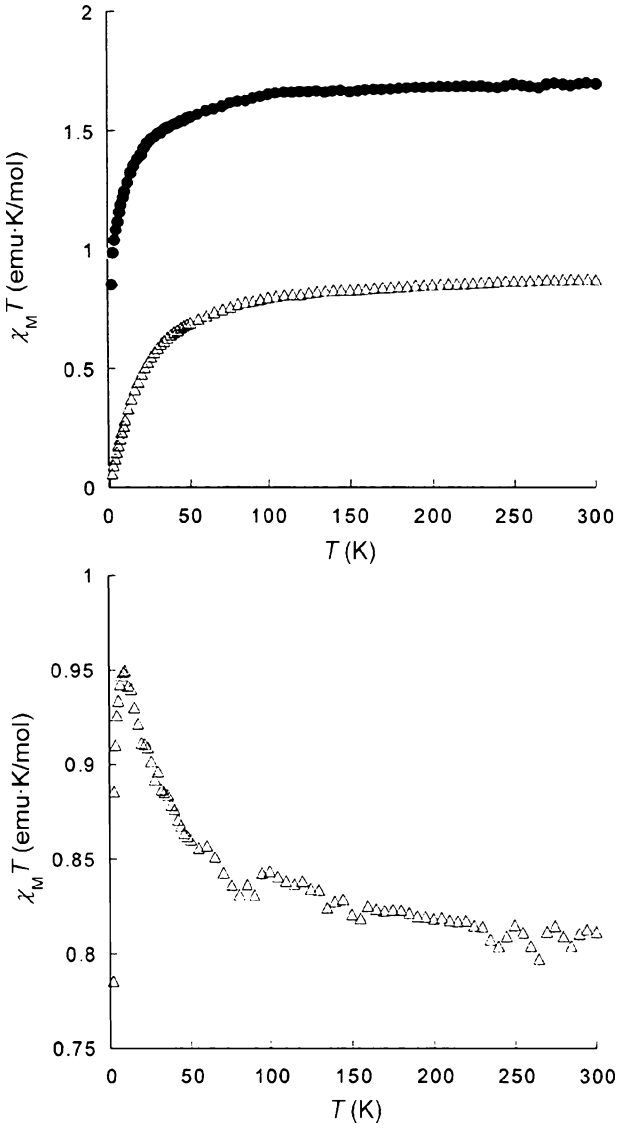

Figure 6. Upper: Variable-temperature magnetic susceptibility data for $UL^7{}_2Cu_2(py)$ (filled circles) and $UL^7{}_2Zn_2(py)$ (open triangles) clusters. Lower: Variable-temperature magnetic susceptibility data ($\Delta\chi_M T$) obtained upon subtraction of the UZn_2 data from the UCu_2 data. Adapted from ref 26b.

momentum, as described above. The $\chi_M T$ data for the UCu_2 cluster exhibit a similar trend, holding constant at 1.7 $cm^3 \cdot K/mol$ down to 100 K before dropping to 0.8 $cm^3 \cdot K/mol$ at 2 K, close to the value of 0.75 $cm^3 \cdot K/mol$ expected for two noninteracting $S = {}^1/_2$ Cu^{II} centers with $g = 2.00$. Subtraction of the UZn_2 data from the UCu_2 data (see Figure 6, lower) removes any contribution from the U^{IV} ion, leaving only the spin contribution of the two Cu^{II} ions together with any vestiges of magnetic exchange coupling. Indeed, the product of the subtracted data sets displays a monotonic rise with decreasing temperature, reaching a maximum at $\Delta\chi_M T = 0.95$ $cm^3 \cdot K/mol$. This increase in $\chi_M T$ is attributed to a ferromagnetic exchange interaction between the U^{IV} and Cu^{II} centers. Although the subtracted data led to the qualitative determination of the sign of the exchange constant ($J > 0$ for ferromagnetic coupling), no attempts to quantify the magnitude of the interaction have been put forth.

While ferromagnetic coupling is observed for $UL^7{}_2Cu_2(py)$, the nature of the exchange appears highly dependent on the identity of the bridging Schiff base and/or number of pyridine molecules coordinated to the copper center, as found upon a comparison of the entire series of UM_2 clusters. For $i = 6$, 8, and 9, behavior similar to that of $UL^7{}_2Cu_2(py)$ was observed, indicative of ferromagnetic coupling. In contrast, for $i = 1-5$, $\Delta\chi_M T$ turns down below 100 K, indicating an antiferromagnetic exchange interaction. The shift from antiferromagnetic to ferromagnetic coupling occurs as the backbone of the Schiff base increases from two C atoms ($i = 1-5$) to three ($i = 6-8$) or four C atoms ($i = 9$). This phenomenon is attributed to an increase in the Cu···U distance, which is associated with a lengthening in the diimino chain. It should be noted, however, that the observation of an increased metal separation is based on the structural characterization of only four UCu_2 clusters ($i = 2$, 6, 7, and 9), for which the average Cu···U distances are 3.538, 3.661, 3.641, and 3.647 Å, respectively. In addition, the magnetic behavior may be affected by other exchange pathways, as evidenced by a downturn in $\chi_M T$ below 15 K observed in the analogous $ThL^i{}_2Cu_2$ clusters ($i = 1$ and 2) and deviation of the magnetization data for $UL^i{}_2Cu_2$ ($i = 1-5$) at 2 K from the Brillouin function. This weak effect is attributed to a long-range intramolecular Cu···Cu interaction and may play an important role in influencing the overall magnetism. In explaining this behavior, the authors note that similar magnetostructural correlations have been documented in gadolinium−transition metal species, where exchange interactions were found to vary with factors such as Cu···Gd distances and dihedral angles between O−Cu−O and O−Gd−O planes.[27]

Analogous trinuclear clusters of the form $UL^7{}_2M_2(py)_2$ (M = Co, Ni, Zn) were prepared to probe the effect of the transition metal on the overall magnetic properties of the cluster.[26a,b,d] Application of the subtraction method to these systems gave $\Delta\chi_M T$ vs T plots that show behavior suggestive of antiferromagnetic coupling between the central U^{IV} ion and the paramagnetic transition metal ions, in contrast to the ferromagnetic coupling exhibited by the UCu_2 cluster. However, as the authors note, spin−orbit effects associated with high-spin Co^{II} centers may complicate the interpretation of the magnetic data for the UCo_2 cluster. Similarly, the downturn in the data for the UNi_2 cluster could potentially be attributed to zero-field splitting associated with the $S = 1$ Ni^{II} centers.

In addition to superexchange interactions, there has been a recent report suggesting that magnetic coupling may occur through direct metal−metal orbital overlap in the mixed-valence linear trinuclear cluster $[UFe^{II}Fe^{III}(C_5H_4NSi(^tBu)Me_2)_4]^+$.[28] This intriguing molecule, prepared through

(27) (a) Benelli, C.; Blake, A. J.; Milne, P. E. Y.; Rawson, J. M.; Winpenny, R. E. P. *Chem.—Eur. J.* **1995**, *1*, 614. (b) Costes, J.-P.; Dahan, F.; Dupuis, A. *Inorg. Chem.* **2000**, *39*, 165. (c) Costes, J.-P.; Dahan, F.; Dupuis, A. *Inorg. Chem.* **2000**, *39*, 5994. (d) Costes, J.-P.; Dahan, F.; Donnadieu, B.; Garcia-Tojal, J.; Laurent, J. P. *Eur. J. Inorg. Chem.* **2001**, 363.

(28) Monreal, M. J.; Carver, C. T.; Diaconescu, P. L. *Inorg. Chem.* **2007**, *46*, 7226.

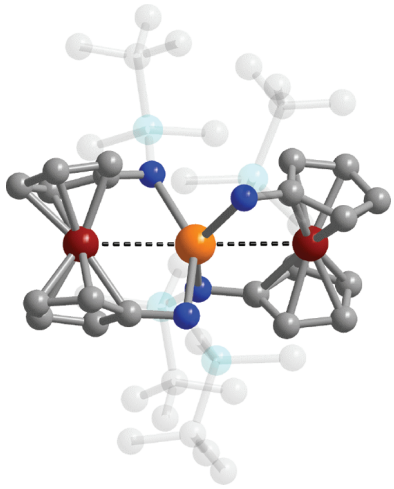

Figure 7. Structure of $[UFe^{II}Fe^{III}(C_5H_4NSi(^tBu)Me_2)_4]^+$.[28] Orange, red, blue, cyan, and gray spheres represent U, Fe, N, Si, and C atoms, respectively. H atoms are omitted for clarity. The $(^tBu)Me_2Si$ groups are drawn transparently for better visualization of the metal coordination environments.

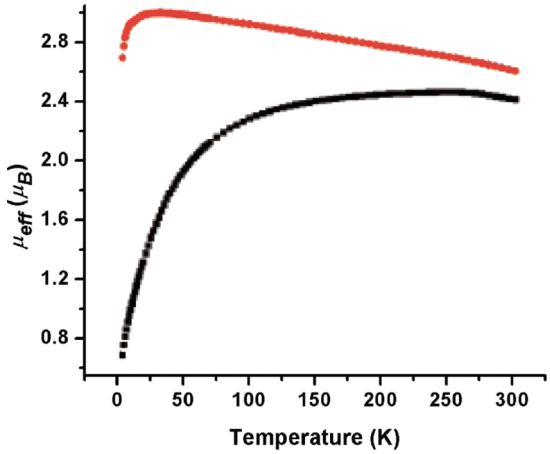

Figure 8. Variable-temperature magnetic data for $UFe^{II}_2(C_5H_4NSi(^tBu)Me_2)_4$ (black squares) and $[UFe^{II}Fe^{III}(C_5H_4NSi(^tBu)Me_2)_4](BPh_4)$ (red circles). Adapted from ref 28.

the one-electron oxidation of $UFe^{II}_2(C_5H_4NSi(^tBu)Me_2)_4$, exhibits a structure consisting of a central U^{IV} ion coordinated to two 1,1′-bis(amido)ferrocenyl derivatives (see Figure 7). Coordination of U^{IV} to the rigid ferrocenylamido moieties enforces U···Fe distances of 2.9556(5) and 2.9686(5) Å.

Variable-temperature magnetic moment measurements show very different behavior for the UFe^{II}_2 and $UFe^{II}Fe^{III}$ clusters (see Figure 8). In the case of the former species, with decreasing temperature, μ_{eff} follows the monotonic drop typical for a U^{IV} center with a $5f^2$ valence electron configuration. In contrast, for the $UFe^{II}Fe^{III}$ cluster, as the temperature is decreased from 300 K, μ_{eff} begins to rise immediately, following a seemingly linear trend before turning over below 20 K. The authors note that the observed behavior is indicative of a magnetic interaction between U^{IV} and Fe^{III} centers. Indeed, the result is without precedent because the spin−orbit coupling and ligand-field effects associated with a paramagnetic uranium center usually give rise to a steady decrease in the net magnetic moment as the temperature is lowered, even in systems exhibiting (weak) ferromagnetic exchange interactions. Thus, the steady increase in μ_{eff} starting at room temperature could be indicative of an extremely strong ferromagnetic exchange interaction mediated by direct orbital overlap between the metals. Note, however, that such a linear upward trend in the moment with decreasing temperature could also potentially arise from complications in applying corrections for the diamagnetic contributions of the unusual sample and/or the sample holder. If indeed the upward trend is the result of a strong ferromagnetic interaction, a simple subtraction of the UFe^{II}_2 data from the $UFe^{II}Fe^{III}$ data would not provide an appropriate means of extracting the pure exchange interaction from the overall magnetism because the added electron imposes a different ligand field on the central U^{IV} ion. Instead, access to a diamagnetic analogue, such as an isostructural species containing Co^{III} in place of Fe^{III}, could perhaps lend itself to the implementation of the subtraction method and estimation of the coupling strength for this interesting system.

Uranium−Radical Systems. Thus far, we have discussed exchange interactions between uranium and other paramagnetic metal centers; however, recent years have seen examples of uranium−radical systems showing evidence of magnetic exchange coupling. Compelling evidence of such an interaction was reported in 2005 in the radical complex $Cp^*_2U^{III}(tpy^{\cdot})$.[29] This molecule, which was prepared through a one-electron reduction of $[Cp^*_2U^{III}(tpy)]I$, features a U^{III} center coordinated by a terpyridyl ligand that houses an additional, delocalized electron. Structural analysis and NMR spectroscopy support the assignments of uranium and ligand oxidation states.

In an attempt to probe the potential exchange between the U^{III} center and the unpaired electron of the reduced ligand, magnetic susceptibility data were collected for both the radical complex and the cationic precursor complex, $[Cp^*_2U^{III}(tpy)]I$. Structural analysis revealed very similar ligand fields for the two species, enabling the use of the subtraction method, wherein the cationic complex data were subtracted from the radical complex data. The resulting $\chi_M T$ data remain essentially constant as the temperature is lowered from 300 K, before decreasing precipitously below 20 K. This interaction is attributed to antiferromagnetic coupling between the $S = {}^3/_2$ U^{III} center and the unpaired electron residing on the reduced terpyridyl ligand. While no attempt was made to quantify the coupling strength, the low temperature at which the drop in $\chi_M T$ is observed indicates that the interaction is relatively weak. One possible explanation for the exchange being weak is the large separation between the unpaired electron and the U^{III} center. While the electron is delocalized throughout the terpyridyl ligand, no good resonance form exists wherein the electron resides on a uranium-coordinated N atom. Alternatively, the drop in $\chi_M T$ may be the result of intermolecular exchange, possibly between radical ligands on neighboring molecules.

A second example of a uranium−radical complex has been found to bind and activate carbon dioxide.[30] This molecule

(29) Mehdoui, T.; Berthet, J.-C.; Thuéry, P.; Salmon, L.; Rivière, E.; Ephritikhine, M. *Chem.—Eur. J.* **2005**, *11*, 6994.
(30) Castro-Rodriguez, I.; Nakai, H.; Zakharov, L. N.; Rheingold, A. L.; Meyer, K. *Science* **2004**, *305*, 1757.

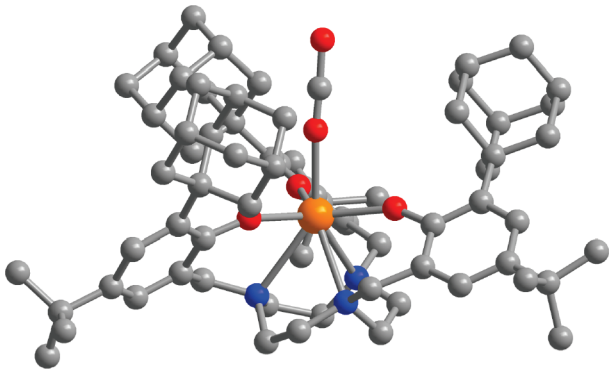

Figure 9. Structure of $((^{Ad}ArO)_3tacn)U(CO_2)$.[30] Orange, red, gray, and blue spheres represent U, O, C and N atoms, respectively. H atoms are omitted for clarity.

was prepared by first encapsulating a U^{III} ion within the pocket of a bulky hexadentate ligand, $(^{Ad}ArO)_3tacn$ [$(^{Ad}ArOH)_3tacn$ = 1,4,7-tris(3-adamantyl-5-*tert*-butyl-2-hydroxybenzyl)-1,4,7-triazacyclonane], to give the electron-rich, coordinatively unsaturated complex $[(^{Ad}ArO)_3tacn]U$. Exposure of this complex to an atmosphere of CO_2 initiates a one-electron transfer from the U^{III} center to the CO_2 ligand to afford $[(^{Ad}ArO)_3tacn]U^{IV}(CO_2)$, as depicted in Figure 9. The structure of the product reveals a remarkable η^1-OCO coordination to the U^{IV} ion, with U−C−O and O−C−O bond angles of 171.1(2)° and 178.0(3)°, respectively. The presence of an unpaired electron residing on the CO_2 carbon was inferred largely from the differences in $C-O_{terminal}$ vs $C-O_U$ bond lengths and shifts in the IR spectra compared to free CO_2, which suggest a bonding scheme comprised of the resonance forms $U^{IV}=O=C^{\bullet}-O^{-} \leftrightarrow U^{IV}-O\equiv C-O^{-}$.

The variable-temperature magnetic susceptibility data for the radical complex were compared to those taken for a related U^{IV} complex, $[(^{Ad}ArO)_3tacn]U^{IV}(N_3)$. At high temperature, the μ_{eff} vs T plots for the two compounds are virtually superimposable.[31] As the temperature is decreased, however, the two curves begin to diverge at ca. 120 K. Below this temperature, the data for the azido complex drop sharply, reaching a minimum of ca. 0.7 μ_B at 5 K. This behavior is consistent with an isolated $5f^2$ U^{IV} center. The low-temperature data for the radical complex display a quite different trend. While the moment drops as the temperature is decreased, it does so more gradually than was observed for the azido analogue and reaches a minimum of ca. 1.5 μ_B at 5 K. The difference in the magnetic behavior in the two complexes is attributed to the extra electron residing on the CO_2 ligand, which accounts for the added magnetic moment at low temperature. However, the observation that the shapes of the two μ_{eff} vs T curves do not deviate above 120 K may suggest the presence of an exchange interaction between the U^{IV} center and the unpaired electron on CO_2. Unfortunately, the subtraction method cannot be applied to this system because of the lack of an analogue of the radical complex that eliminates the radical but preserves the ligand field experienced by uranium. Thus, it seems unlikely that any exchange interactions between the two paramagnetic centers can be wholly extracted from the overall magnetic behavior of the molecule.

Recently, it was found that a related U^{III} species could reduce di-*tert*-butylbenzophenone to give $[((^{t\text{-}Bu}ArO)_3tacn)U^{IV}(OC^{\bullet t\text{-}Bu}Ph_2)]$.[32] The crystal data and the results of density functional theory (DFT) calculations are consistent with an overall structure comprised of four resonance forms, three containing a U^{IV} center with an unpaired electron residing on the di-*tert*-butylbenzophenone fragment, and one featuring a U^{III} center bound to a diamagnetic di-*tert*-butylbenzophenone. The temperature dependence of the magnetic susceptibility data for this radical complex shows a trend similar to that of the CO_2 complex, with the exception of a higher moment at 300 K, which is attributed to a contribution from the U^{III} resonance form (see Figure S1 in the Supporting Information). Calculations suggest that coupling between the U^{IV} center and the radical ligand is at least physically reasonable because the computed singly occupied molecular orbital of the molecule possesses both metal and ligand character.

Modular Approach to the Synthesis of Halide-Bridged Actinide−Transition Metal Clusters

Motivated by the successes achieved and challenges encountered in the work presented above, our research has focused on the development of a modular strategy for synthesizing halide-bridged 5f−3d clusters.[19,33] This effort was spurred by our preparation of the pyrazolate-bridged dimer complex $[U(Me_2Pz)_4]_2$, obtained from the reaction of UCl_4 with $K(Me_2Pz)$ (Me_2Pz^{-} = 3,5-dimethylpyrazolate). Initial reactivity studies of this molecule revealed its susceptibility to cleavage by bases such as tetrahydrofuran (THF) via displacement of the bridging pyrazolate ligands. Of particular significance was the finding that the dimer could be cleaved analogously by the terminal chloride ligand of a transition metal complex to afford a chloride-bridged cluster. Thus, insertion of the *trans*-dichloro complexes (cyclam)MCl_2 (cyclam = 1,4,8,11-tetraazacyclotetradecane; M = Co, Ni, Cu, Zn) was found to generate the linear trinuclear species (cyclam)$M[(\mu\text{-}Cl)U(Me_2Pz)_4]_2$, as represented in Figure 10. Similar to the $UL^i{}_2M_2(py)_n$ clusters discussed above, this MU_2 system is well-suited for probing the possibility of magnetic exchange coupling, owing to the invariance in the coordination geometry of the U^{IV} centers as the central M atom is changed. Importantly, the existence of the ZnU_2 member of the series, featuring an $S = 0$ Zn^{II} center, enables subtraction of the spin−orbit and ligand-field effects associated with the U^{IV} centers. The subtraction procedure utilized is identical with that described in detail above.

(31) Note that $\chi_M T$ provides a sensitive measure of the magnetic moment of a sample and is related to the perhaps more familiar quantity μ_{eff} as follows: $\mu_{eff} = (8\chi_M T)^{1/2}\mu_B$.

(32) Lam, O. P.; Anthon, C.; Heinemann, F. W.; O'Connor, J. M.; Meyer, K. *J. Am. Chem. Soc.* **2008**, *130*, 6567.

(33) Rinehart, J. D.; Bartlett, B. M.; Kozimor, S. A.; Long, J. R. *Inorg. Chim. Acta* **2008**, *361*, 3534.

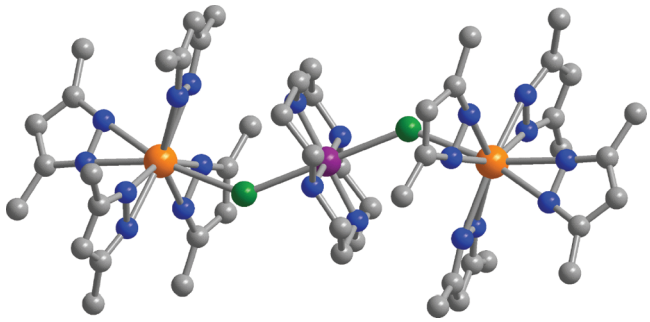

Figure 10. Structure of the linear cluster (cyclam)Co[(μ-Cl)U(Me_2Pz)$_4$]$_2$.[33] Orange, purple, green, gray, and blue spheres represent U, Co, Cl, C, and N atoms, respectively. H atoms are omitted for clarity.

Analysis of the magnetic behavior of (cyclam)Co[(μ-Cl)U(Me_2Pz)$_4$]$_2$ (CoU_2) leads to what is perhaps the most clear-cut case to date for magnetic exchange coupling between an actinide ion and a transition metal ion. Figure 11 shows the variation in $\chi_M T$ with temperature for the CoU_2 and ZnU_2 clusters. Inspection of the data shows that the two species exhibit behavior similar to that of other molecules containing U^{IV} centers with a $5f^2$ valence electron configuration. At room temperature, the $\chi_M T$ values of 2.06 cm^3·K/mol for ZnU_2 and 2.47 cm^3·K/mol for CoU_2 are reasonable for the uncoupled constituent metal centers for each system, with the difference of 0.41 cm^3·K/mol being attributable to the presence of a low-spin Co^{II} center with $S = {}^1/_2$ in the CoU_2 species. At low temperature, $\chi_M T$ tends toward zero for the ZnU_2 cluster, as expected for depopulation of the upper U^{IV} Stark sublevels. With decreasing temperature, the data for the CoU_2 cluster also drop steadily, but with a rather different curvature. This difference in curvature is reflected best in the $\Delta\chi_M T$ values obtained upon subtraction of the ZnU_2 data from the CoU_2 data. In distinct contrast to the data obtained for the mononuclear complex (cyclam)$CoCl_2$, for which $\chi_M T$ remains essentially constant at 0.41 cm^3·K/mol, $\Delta\chi_M T$ increases monotonically as the temperature is lowered, reaching a maximum of 0.68 cm^3·K/mol at 40 K before turning over. It is this rise in $\Delta\chi_M T$ that indicates the presence of ferromagnetic exchange coupling between the U^{IV} and Co^{II} centers within the CoU_2 cluster. The downturn in $\Delta\chi_M T$ below 40 K can be attributed to a loss of the exchange coupling due to reduction of the total angular momentum of the U^{IV} centers upon depopulation of the Stark sublevels. Note that this effect appears to be universal in the ferromagnetically coupled uranium systems studied so far using the subtraction method (see Figures 6 and 11).

In view of the significant rise observed in the $\Delta\chi_M T$ data for the CoU_2 cluster, efforts were made to quantify the strength of the magnetic exchange interaction.[33] This is not at all straightforward because the exchange will be significantly attenuated by the gradual loss of coupling strength due to angular momentum depletion on the U^{IV} centers as the temperature is lowered. Nevertheless, a lower bound for the exchange constant, J, can be obtained by fitting the data assuming that no loss of coupling strength occurs with decreasing temperature. Working under this assumption, a temperature-invariant contribution of 2.00 cm^3·K/mol was

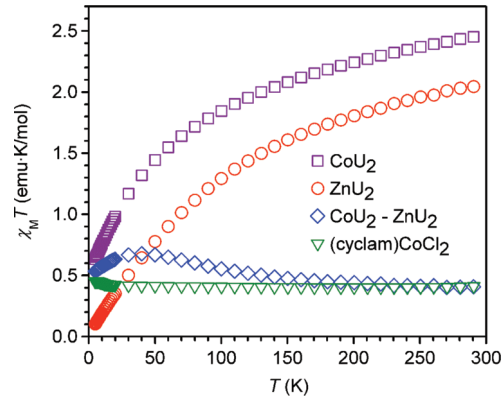

Figure 11. Variable-temperature magnetic susceptibility data for the trinuclear cluster (cyclam)Co[(μ-Cl)U(Me_2Pz)$_4$]$_2$ (CoU_2, purple squares) and (cyclam)Zn[(μ-Cl)U(Me_2Pz)$_4$]$_2$ (ZnU_2, red circles).[33] Blue diamonds correspond to a subtraction of the ZnU_2 data from the CoU_2 data. Magnetic data for the precursor complex (cyclam)$CoCl_2$ are depicted as green triangles.

added to the $\Delta\chi_M T$ data to account for a spin-only ($S = 1$) contribution from each of the two U^{IV} centers. The resulting data are shown at the top of Figure 12 and were fit using MAGFIT 3.1[34] and an exchange Hamiltonian of the following form.

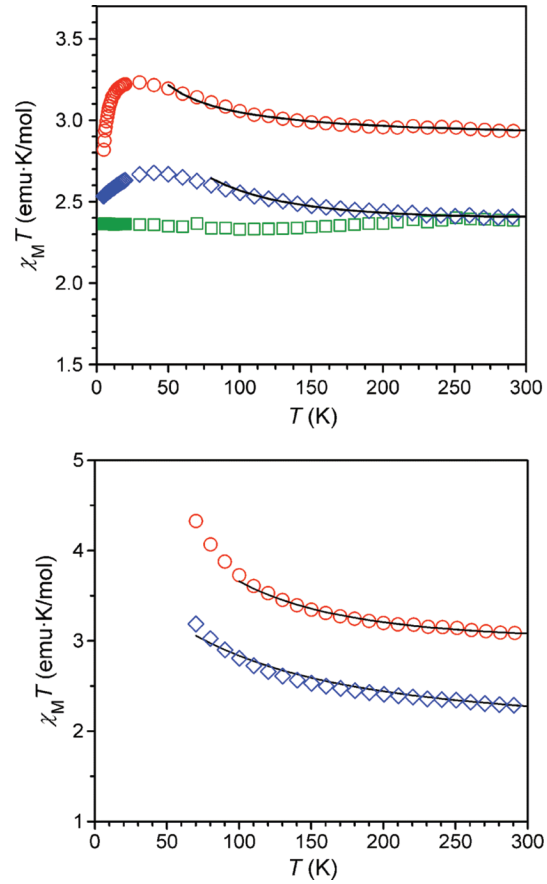

Figure 12. Adjusted $\chi_M T$ data used to estimate the bounds on the strength of the magnetic exchange coupling in the CoU_2 (red circles), NiU_2 (blue diamonds), and CuU_2 (green squares) clusters.[19,33] Black lines represent calculated fits to the data. Upper: $\Delta\chi_M T$ data for $\chi_M T(CoU_2) - \chi_M T(ZnU_2)$, $\chi_M T(NiU_2) - \chi_M T(ZnU_2)$, and $\chi_M T(CuU_2) - \chi_M T(ZnU_2)$ used to obtain a lower bound. A value of 2.00 cm^3·K/mol has been added to represent a spin-only contribution from each of the two U^{IV} centers. Lower: $\chi_M T$ data obtained upon multiplication by the reduction function $r(T) = (2.00$ cm^3·K/mol$)/\chi_M T(ZnU_2)$ and used to obtain an upper bound.

$$\hat{H} = -2J[\hat{S}_{Co} \cdot (\hat{S}_{U(1)} + \hat{S}_{U(2)})] \quad (2)$$

The spin-only nature of this Hamiltonian reflects the empirical excision of the U^{IV}single-ion effects. Note also that only the data above 70 K were fit because below this temperature significant loss of the angular momentum on the U^{IV} centers depletes the effects of the magnetic exchange coupling. The best fit affords a lower bound of $J_{min} = 15$ cm^{-1}. On the contrary, if it is assumed that the entire drop in $\chi_M T$ for the ZnU_2 cluster with decreasing temperature is caused by a loss of the angular momentum at the U^{IV} centers, then we can obtain an upper bound for the exchange constant of the CoU_2 cluster. Here, the deviation of $\chi_M T$ for ZnU_2 from the spin-only value of 2.00 cm^3·K/mol is encompassed in an empirical function, $r(T) = (2.00$ cm^3·K/mol)/$\chi_M T$. For example, at 5 K, $\chi_M T$ for ZnU_2 is 0.104 cm^3·K/mol, giving a reduction factor of $r = 19.183$. Multiplying the measured $\chi_M T$ data for the CoU_2 cluster by the function $r(T)$ determined for the ZnU_2 cluster, we can then adjust the CoU_2 data for any variation in the magnetic susceptibility due to the individual U^{IV} centers. Any deviation from the room temperature $\chi_M T$ value of 2.375 cm^3·K/mol should be attributable to exchange coupling between the U^{IV} and Co^{II} centers. The data generated using this reduction factor technique are shown in blue at the bottom of Figure 12. Again when only the data above 70 K and the spin Hamiltonian given in eq 2 are employed, the best fit resulted in an upper bound of $J_{max} = 48$ cm^{-1}. Thus, the exchange constant lies bracketed within the range 15 cm$^{-1} \leq J \leq 48$ cm^{-1}.

It is, of course, of interest to understand the origin of this ferromagnetic coupling within the CoU_2 cluster. A DFT calculation performed on a $[(Me_2Pz)_4UCl]^-$ fragment of the cluster revealed the unpaired electrons of the U^{IV} center to reside in the $5f_{xyz}$ and $5f_{z(x^2-y^2)}$ orbitals.[19,35] Importantly, these orbitals have δ symmetry with respect to the U−Cl bond, such that the overlap with σ and π orbitals of the chloride bridge will be zero. Any of the spin from the Co^{II} $3d_{z^2}$ orbital feeding through the chloride bridging ligands will therefore engage rigorously orthogonal orbitals, leading to a ferromagnetic exchange interaction. Consistently, ferromagnetic exchange is also observed for the NiU_2 cluster, which features an $S = 1$ Ni^{II} center with unpaired electrons in the $3d_{z^2}$ and $3d_{x^2-y^2}$ orbitals. In this case, however, fits to the data suggest somewhat weaker exchange, with 2.8 cm$^{-1} \leq J \leq 19$ cm^{-1} (see Figure 12). The attenuation can perhaps be explained by the increased effective nuclear charge experienced by the $3d_{z^2}$ electron of the Ni^{II} center. Also consistent with a superexchange model, the $\Delta\chi_M T$ data for the CuU_2 cluster are essentially invariant with temperature, indicating the complete absence of magnetic exchange coupling (see Figure 12, upper). This result can be understood as arising from the strict orthogonality between the σ and π orbitals of the chloride bridge and the $3d_{x^2-y^2}$ orbital containing the sole unpaired electron of the Co^{II} center.

(34) Schmitt E. A. Ph.D. Thesis, University of Illinois at Urbana−Champaign, 1995.

(35) We have assumed that the z axis is oriented along the U−Cl or M−Cl bond.

Table 1. Exchange Constants and Other Fit Parameters Obtained for $UL^i_2Cu_2(py)$ Clusters

	J_{min} (cm^{-1})	g	TIP ($\times 10^{-6}$ cm^{-1})
$UL^1_2Cu_2(py)$	−1.5	2.00	557
$UL^2_2Cu_2(py)$	−0.8	2.06	0
$UL^3_2Cu_2(py)$	−1.8	2.05	274
$UL^4_2Cu_2(py)$	−0.5	2.04	243
$UL^5_2Cu_2(py)$	−1.3	1.99	619
$UL^6_2Cu_2(py)$	+2.6	1.99	191
$UL^7_2Cu_2(py)$	+0.8	2.04	108
$UL^8_2Cu_2(py)$	+0.7	2.02	85
$UL^9_2Cu_2(py)$	+1.9	2.04	112

The relatively strong ferromagnetic coupling observed for the CoU_2 cluster suggests that, were it not for U^{IV} angular momentum reduction arising from depopulation of the Stark sublevels, the CoU_2 cluster would display highly correlated ferromagnetic behavior at low temperature. Indeed, with $J \geq 15$ cm^{-1}, this molecule is the first indicating that the exchange interaction between an actinide ion and a transition metal ion can be stronger than has been quantified to date for the exchange between a lanthanide ion and a transition metal ion (typically $J < 4$ cm^{-1}).[6d] This cluster does not, however, exhibit the slow magnetic relaxation indicative of a SMM. For such a purpose, it is, of course, of interest to examine other potential high-spin systems exhibiting strong magnetic exchange coupling. We have therefore also applied our fitting methods to the $\Delta\chi_M T$ data reported for the $UL^i_2Cu_2(py)$ clusters discussed earlier (see Figures S2 and S3 in the Supporting Information).[26] As summarized in Table 1, the results afford lower bounds for the exchange constants that climb as high as $J_{min} = 2.6$ cm^{-1} for the $UL^6_2Cu_2(py)$ species. Hence, species involving the L^6 ligand in particular might provide a good starting point for further exploration of this system.

The synthetic route used to isolate the (cyclam)M[(μ-Cl)U$(Me_2Pz)_4$]$_2$ linear trinuclear clusters presents a number of possible means for enhancing the magnitude of the exchange coupling and the spin of the ground state in actinide-containing molecules by providing control over many electronic factors that affect magnetic exchange. For example, the $[U(Me_2Pz)_4]_2$ dimer can likely be cleaved by many compounds to form new coordination clusters, which will enable the judicious examination of actinide magnetic exchange as a function of the identity of the central metal ion as well as the bridging ligand. In addition, more subtle electronic "fine-tuning" may be available through variation of substituents on the pyrazolate ancillary ligand. We therefore report here our initial efforts to explore the generality of the synthetic approach used to form trinuclear clusters, as well as new uranium complexes with electron-withdrawing pyrazolate ligands.

Because the reaction that provided the MU_2 (M = Co, Ni, Cu, Zn) clusters has only been achieved with late transition metals, possible routes to related clusters containing early-to-middle transition metal chlorides were investigated. Given the large number of complexes of the type $(dmpe)_2MX_2$,[36] it seemed that the reaction of $[U(PzMe_2)_4]_2$ with such species might demonstrate the versatility of coordination chemistry available to the dimer. Indeed, stoichiometric addition of $(dmpe)_2FeCl_2$[36a] to $[U(Me_2Pz)_4]_2$

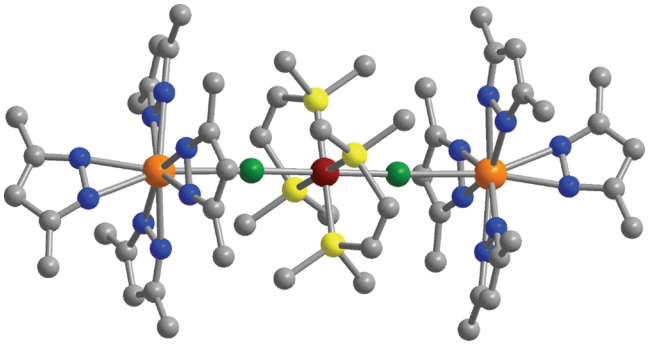

Figure 13. Structure of the linear cluster $(dmpe)_2Fe[(\mu\text{-}Cl)U(Me_2Pz)_4]_2$ (**1**). Orange, dark red, green, pink, gray, and blue spheres represent U, Fe, Cl, P, C, and N atoms, respectively. H atoms are omitted for clarity.

resulted in the formation of the new linear trinuclear cluster $(dmpe)_2Fe[(\mu\text{-}Cl)U(Me_2Pz)_4]_2$ (**1**). This cluster, depicted in Figure 13, is equivalent in its connectivity to the cyclam-containing species but displays a more linear Fe−Cl−U bridge angle of 168.8(2)°. Magnetic susceptibility data are consistent with the expected low-spin $S = 0$ electron configuration for the Fe^{II} center. Thus, this species should serve as a diamagnetic analogue for the evaluation of isostructural $(dmpe)_2M[(\mu\text{-}Cl)U(Me_2Pz)_4]_2$ clusters where M is paramagnetic, in analogy to the ZnU_2 complexes previously discussed.

Encouraged by the formation of **1**, we examined the reactivity of $(dmpe)_2MCl_2$ (M = V, Cr) complexes for evidence of similar cluster formation. However, a surprisingly different reaction chemistry was observed. The $(dmpe)_2MCl_2$ (M = V, Cr) complexes indeed react with $[U(Me_2Pz)_4]_2$ but not to form trinuclear clusters. Instead, abstraction of dmpe by the U^{IV} centers occurs to generate the one-dimensional chain compound $(Me_2Pz)_4U(\mu\text{-}dmpe)$ (**2**), as shown in Figure 14. This is unusual, given that phosphines are generally thought to be poor ligands for tetravalent uranium and that they form relatively stable complexes with V^{II} and Cr^{II}.

In an effort to prevent ligand abstraction by the U^{IV} centers, reactions between $[U(PzMe_2)_4]_2$ and $(dppe)_2MCl_2$ [M = V, Mn, Fe, Co;[37] dppe = bis(diphenylphosphino)ethane] were investigated because the softer and more sterically demanding dppe ligand was expected to have less affinity for U^{IV}. In solution, ^1H NMR spectroscopy showed no evidence for the formation of trinuclear clusters or of dppe abstraction, except in the case of $(dppe)_2MnCl_2$. In this case, ligand abstraction occurs, providing the dinuclear complex $[(Me_2Pz)_4U]_2(\mu\text{-}dppe)$ (**3**), exhibiting the dppe-bridged structure depicted in Figure 15. Given its varied reactivity with $(dppe)_2MCl_2$ and $(dmpe)_2MCl_2$ to form either bridging halide or bridging phosphine complexes, $[U(PzMe_2)_4]_2$ clearly supports a

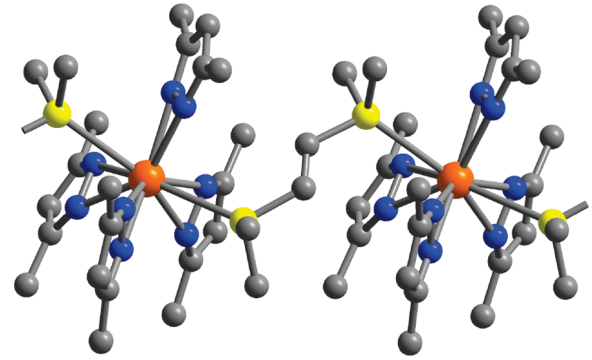

Figure 14. Structure of a portion of the one-dimensional chain compound $(Me_2Pz)_4U(\mu\text{-}dmpe)$ (**2**). Orange, yellow, gray, and blue spheres represent U, P, C, and N atoms, respectively. H atoms are omitted for clarity.

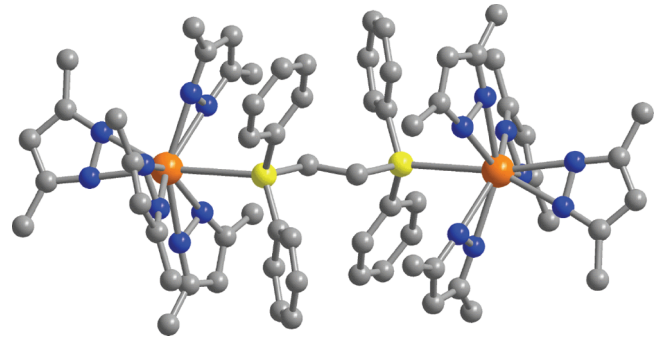

Figure 15. Structure of the dinuclear complex **3**. Orange, yellow, gray, and blue spheres represent U, P, C, and N atoms, respectively. H atoms are omitted for clarity.

diverse cluster chemistry that, provided the right bridging ligands, may even offer opportunities for the formation of higher-nuclearity clusters.

Another level of control within such systems can potentially be attained through utilization of electron-withdrawing substituents on the pyrazolate ligands. In particular, more electron-withdrawing pyrazolate ligands should enhance the halophilicity of the U^{IV} centers, while also potentially adjusting their propensity for engaging in magnetic exchange coupling. Along these lines, 4 equiv of 3,4,5-(tribromo)pyrazolate or 3,5-bis(trifluoromethyl)pyrazolate readily react with $UI_3(THF)_4$ to form **4** and **5**, respectively (see Figure 16). In these complexes, the $(Br_3Pz)^-$ and $[(CF_3)_2Pz]^-$ ligands appear to enhance the Lewis acidity of the U^{IV} center because **4** and **5** coordinate two THF molecules, while the reaction between $[U(PzMe_2)_4]_2$ and THF results in the mono-THF adduct $(Me_2Pz)_4U(THF)$.[19] The altered electronic properties of these new systems will likely provide selectivity for the coordination of hard bridging ligands and prevent the abstraction of soft ancillary ligands during cluster formation.

A number of other modifications to the $(cyclam)M[(\mu\text{-}Cl)U(Me_2Pz)_4]_2$ system are worthy of pursuit. Substitution of fluoride, bromide, or iodide for the bridging chloride ligand can be expected to have a significant impact on the strength of the magnetic exchange interactions, with the heavier bridges likely leading to increased coupling. Replacement of the U^{IV} centers with other An^{IV} centers via the synthesis and implementation of dimeric complexes of the type $[An(Me_2Pz)_4]_2$ would enable the study of how variation of the number and radial extension of the 5f electrons effects

(36) (a) Girolami, G. S.; Wilkinson, G.; Galas, A. M. R.; Thornton-Pett, M.; Hursthouse, M. B. *J. Chem. Soc., Dalton Trans.* **1985**, 1339. (b) Fong, L. K.; Fox, J. R.; Foxman, B. M.; Cooper, N. J. *Inorg. Chem.* **1986**, *25*, 1880. (c) Saboonchian, V.; Wilkinson, G.; Hussain-Bates, B.; Hursthouse, M. B. *Polyhedron* **1991**, *10*, 595. (d) Protasiewicz, J. D.; Bianconi, P. A.; Williams, I. D.; Lui, S.; Rao, C. P.; Lippard, S. J. *Inorg. Chem.* **1992**, *31*, 4134.

(37) (a) Schmid, G.; Noeth, H. *Z. Naturforsch., B* **1965**, *20*, 1008. (b) Aresta, M.; Giannoccaro, P.; Rossi, M.; Sacco, A. *Inorg. Chim. Acta* **1971**, *5*, 115. (c) Holt, D. G. L.; Larkworthy, L. F.; Povey, D. C.; Smith, G. W.; Leigh, G. J. *Inorg. Chim. Acta* **1993**, *207*, 11.

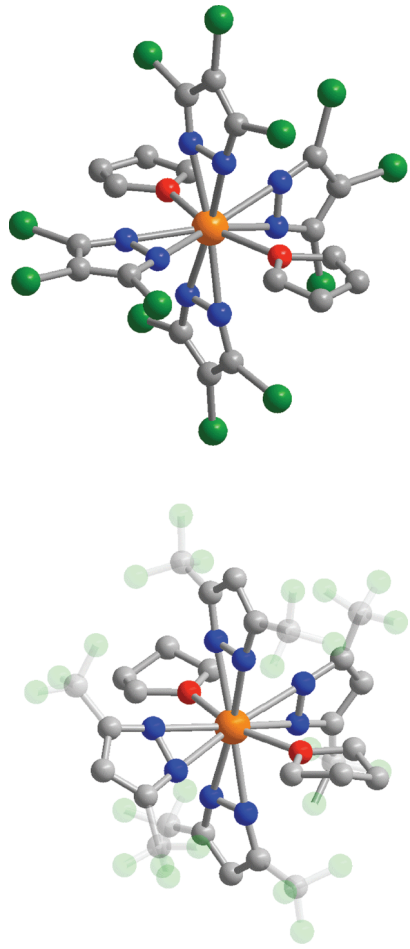

Figure 16. Structures of the molecular complexes **4** (top) and **5** (bottom). Orange, dark-green, gray, blue, and light-green spheres represent U, Br, C, N, and F atoms, respectively. H atoms are omitted for clarity. The CF_3 groups at the 3 and 5 positions of the pyrazolate ligands are rendered transparently for better visualization.

coupling. Of particular interest are actinide ions such as Np^{IV}, for which an odd electron count would prevent complete loss of the total angular momentum, even at very low temperatures, enabling access to high-spin ground states. Such experiments, of course, require that one have the facilities to work with highly radioactive elements. An alternative means of ensuring an odd 5f electron count would be to develop similar modular systems that stabilize uranium in the 3+ oxidation state. This approach would likely have the added benefit of increasing the strength of the exchange interactions, owing to the more diffuse 5f orbitals of the U^{III} centers. Finally, one could envision using a similar synthetic approach to generate bent trinuclear clusters incorporating *cis*-dichloro complexes, or even, through the use of transition metal complexes bearing more than two terminal chloride ligands, higher-nuclearity clusters with a higher potential total spin.

Conclusions and Outlook

Targeted assembly of simple, low-nuclearity clusters has been and continues to be the key to unraveling the complex interactions that give rise to magnetic exchange coupling in actinide-containing molecules. The results presented here suggest that access to carefully designed systems can serve to excise spin−orbit coupling and ligand-field effects from the magnetic susceptibility data for such species. By assuming that all or none of the decay in the magnetic susceptibility is due to diminished exchange coupling stemming from a reduction of U^{IV} ion angular momentum, methods have been developed for estimating upper and lower bounds for the exchange constant. Among the systems that can be treated in this way, the linear trinuclear cluster (cyclam)Co[(μ-Cl)U($Me_2Pz)_4]_2$ provides an initial demonstration that strong ferromagnetic exchange coupling, with 15 $cm^{-1} \leq J \leq 48$ cm^{-1}, can be achieved between an actinide ion and a transition metal ion. While the range for J calculated by this method is large, the lower bound of $J = 15$ cm^{-1} is certainly great enough to validate the idea that significant concerted magnetic behavior can arise in molecular clusters containing actinide elements. The modular synthetic approach employed thus far provides numerous opportunities for manipulating the strength of the magnetic exchange coupling, the total number of unpaired electrons, and perhaps even the 5f electron count. Ultimately, we hope that the data from these systems will be of utility in the development of electronic structure models that successfully describe the magnetic behavior of actinide-containing molecules. In addition, it is envisioned that, by building upon these results, the combination of strong magnetic exchange coupling and a large orbital angular momentum might lead to new single-molecule magnets.

Experimental Section

General Considerations. The syntheses and manipulations of the extremely air- and moisture-sensitive compounds described below were conducted under N_2 with rigorous exclusion of air and water by Schlenk and glovebox techniques. THF was distilled over sodium and benzophenone. Toluene and dichloromethane were saturated with N_2, passed through an activated alumina column, degassed by three freeze−pump−thaw cycles, and stored under N_2 over 3 Å molecular sieves. Toluene-d_8 and C_6D_6 (Cambridge Isotope Laboratories) were distilled over a NaK alloy and benzophenone and were degassed by three freeze−pump−thaw cycles. Methanol was distilled over magnesium and iodine and saturated with N_2. The compounds $(dmpe)_2MCl_2$ (M = V, Cr, Fe),[36a] UI_3,[38] $[U(Me_2Pz)_4]_2$,[19] and (cyclam)M[(μ-Cl)U($Me_2Pz)_4]_2$ (M = Zn, Ni, Cu, Co)[19,33] were synthesized as previously described. The complex $(dppe)_2MnCl_2$ was prepared by stirring $MnCl_2$ and dppe at 60 °C for 24 h in methanol. The filtrate was isolated, washed with methanol, and dried under vacuum. NMR spectra were collected using Bruker 300, 400, and 500 MHz spectrometers. IR spectra were obtained using KBr pellets and were recorded on a Nicolet Avatar 360 FTIR spectrometer. UV−vis absorption spectra were measured using quartz cuvettes equipped with Teflon-sealable stopcocks and were recorded on a Hewlett-Packard 8453 spectrophotometer. Elemental analyses were performed by the analytical laboratories at the University of California, Berkeley. Single-crystal X-ray structure determinations were performed on a Brüker APEX diffractometer. Crystals were mounted on Kapton loops and cooled under a N_2 stream. The *SMART*[39] program package was used to

(38) Cloke, F. G. N.; Hitchcock, P. B. *J. Am. Chem. Soc.* **2002**, *124*, 9352.
(39) *SMART Software Users Guide*, version 5.1; Bruker Analytical X-ray Systems, Inc.: Madison, WI, 1999.

determine the unit cell parameters and for data collection (30 s/frame scan time for a hemisphere of diffraction data). Data integration was performed by *SAINT*[40] and the absorption correction provided by *SADABS*.[41] Subsequent calculations were carried out using the *SHELXTL* program.[42] The structures were solved by direct methods and refined on F^2 by full-matrix least-squares techniques. The analytical scattering factors for neutral atoms[43] were used throughout the analysis. H atoms were included using a riding model.

(dmpe)$_2$Fe[(μ-Cl)U(Me$_2$Pz)$_4$]$_2$ (1). Toluene (5 mL) was added to a flask charged with (dmpe)$_2$FeCl$_2$ (146 mg, 0.342 mmol), and the resulting suspension was heated at 90 °C until a transparent green solution was obtained. The hot solution was added dropwise to a green solution of [U(Me$_2$Pz)$_4$]$_2$ (428 mg, 0.346 mmol) in toluene (5 mL), and the resulting solution was stirred for 12 h at room temperature. The solution was filtered through Celite, concentrated under reduced pressure to a volume of ca. 1 mL, and cooled to −25 °C. After 24 h, the supernatant solution was decanted, and the crystals that had formed were collected and dried under reduced pressure. A small number of large, dark-green cube-shaped crystals of (dmpe)$_2$FeCl$_2$ were separated manually to give 220 mg (39%) of product as yellow-green plate-shaped crystals. Crystals suitable for X-ray analysis were obtained upon cooling a hot toluene solution to −25 °C. ^{1}H NMR (C_6D_6, 298 K): δ −6.0 (s, 24, *Me*-dmpe, $\Delta\nu_{1/2}$ = 700 Hz), 6.3 (s, 48, *Me*$_2$Pz, $\Delta\nu_{1/2}$ = 1300 Hz) ppm. Resonances attributable to the methylene protons of the dmpe ligand and the ring protons of $(Me_2HCN_2)^-$ were not identifiable. IR: 3200w, 3099w, 2964m, 2945m, 2921s, 2905s, 2870m, 2805w, 2720w, 1570w, 1520s, 1457s, 1435s, 1417s, 1384m, 1372m, 1363m, 1324m, 1310m, 1302m, 1288m, 1235w, 1153w, 1105m, 1077w, 1053m, 1027m, 1007s, 958s, 941s, 929s, 915m, 893m, 843m, 782s, 740m, 731s, 710m, 649m, 586w, 564w cm^{-1}. Absorption spectrum (CH_2Cl_2): λ_{max} 310 (sh), 489, 517, 564, 614, 622 (sh), 679, 809, 867, 929 (sh), 1002 (sh), 1046 nm. Anal. Calcd for $C_{52}H_{88}Cl_2FeN_{16}P_4U_2$: C, 37.55; H, 5.29; N, 13.48. Found: C, 37.61; H, 5.62; N, 13.55.

(Me$_2$Pz)$_4$U(μ-dmpe) (2). A colorless solution of dmpe (59 mg, 0.39 mmol) in 5 mL of toluene was added to a green solution of [U(Me$_2$Pz)$_4$]$_2$ (240 mg, 0.20 mmol) in 5 mL of toluene, affording a green precipitate. The suspension was stirred for 24 h and filtered. The filtrate was concentrated to a volume of ca. 5 mL under reduced pressure, heated until the small amount of green preciptate dissolved, and cooled to −25 °C. After 24 h, the solvent was decanted and the green needle-shaped crystals that had formed were dried under reduced pressure to give 74 mg (25%) of product. Crystals suitable for X-ray analysis were obtained upon cooling a hot toluene solution to −25 °C. ^{1}H NMR (C_6D_6, 298 K): δ −17.4 (s, 4H, C*H*$_2$-dmpe, $\Delta\nu_{1/2}$ = 190 Hz), −10, (s, 12H, *Me*-dmpe, $\Delta\nu_{1/2}$ = 75 Hz), 5.4 (s, 24H, *Me*$_2$Pz, $\Delta\nu_{1/2}$ = 190 Hz), 16.8 (s, 4H, C*H*-Me$_2$Pz, $\Delta\nu_{1/2}$ = 120 Hz) ppm. IR: 3202w, 3132w, 3100m, 2963s, 2920s, 2896w, 2805m, 2716w, 1569m, 1514s, 1409bs, 1373s, 1364s, 1310m, 1288s, 1274m, 1180w, 1154w, 1104s, 1051m, 1029m, 1009s, 961s, 945s, 903s, 868m, 840w, 828w 786s, 768s, 731s, 698w, 678w, 661w, 651w, 646w, 585w, 563m, 433s cm^{-1}. Absorption spectrum (toluene): λ_{max} 332 (sh), 437, 462 (sh), 477, 519, 532 (sh), 571, 616, 623 (sh), 630 (sh), 668, 679, 808, 867, 939 (sh), 1003 (sh), 1044 nm. Anal. Calcd for $C_{26}H_{44}N_8P_2U$: C, 40.64; H, 5.73; N, 14.59. Found: C, 40.63; H, 5.72; N, 14.43.

[(Me$_2$Pz)$_4$U]$_2$(μ-dppe) (3). A solution of [U(Me$_2$Pz)$_4$]$_2$ (0.150 g, 0.121 mmol) in 5 mL of dichloromethane was added to a solution of dppe (0.483 g, 0.121 mmol) in 5 mL of dichloromethane. The resulting green solution was stirred for 24 h and filtered through Celite. The filtrate was concentrated to saturation under reduced pressure and cooled to −25 °C. After 3 days, colorless block-shaped crystals of dppe had formed. After an additional 18 days, yellow-green rod-shaped crystals of product had formed, as identified by single-crystal X-ray analysis. Further characterization of this compound was hindered by a low yield and the concurrent crystallization of dppe.

(Br$_3$Pz)$_4$U(THF)$_2$·0.5PhMe (4·0.5PhMe). A pale-yellow solution of K(Br$_3$Pz) (0.444 g, 1.29 mmol) in 6 mL of THF was added dropwise to a stirred purple solution of UI$_3$ (0.200 g, 0.323 mmol) in 4 mL of THF, resulting in a brown slurry. After stirring for 36 h, the mixture was filtered through a 0.22-μm-pore nylon disk to remove a gray solid. The solvent was removed from the brown filtrate in vacuo to give an oily brown residue. The residue was extracted into 4 mL of toluene, and the resulting brown mixture was filtered through Celite to remove a small amount of an insoluble brown solid. The dark-yellow filtrate was cooled to −25 °C, whereupon yellow-green block-shaped crystals formed after 5 days. The crystals were collected by vacuum filtration and washed with toluene (2 × 1 mL), which had been chilled to −25 °C, to give 0.136 g (26%) of product. Anal. Calcd for $C_{23.5}H_{20}Br_{12}N_8O_2U$: C, 17.18; H, 1.23; N, 6.82. Found: C, 17.98; H, 1.20; N, 7.11.

[(CF$_3$)$_2$Pz]$_4$U(THF)$_2$ (5). A yellow solution of K[(CF$_3$)$_2$Pz] (371 mg, 1.65 mmol) in 5 mL of THF (5 mL) was added dropwise to a stirred purple solution of UI$_3$ (255 mg, 0.412 mmol) in 5 mL of THF, resulting in the immediate formation of a brown slurry. After stirring for 48 h, the mixture was filtered through a 0.22-μm-pore nylon disk under reduced pressure to remove a gray solid. The solvent was removed from the brown filtrate in vacuo to afford an oily brown residue. The residue was extracted into 4 mL of toluene, and the resulting brown mixture was filtered through Celite to remove a small amount of brown solid. The brown filtrate was cooled to −25 °C, whereupon brown block-shaped crystals formed after 4 days. The crystals were collected by filtration and washed with toluene (2 × 1 mL), which had been chilled to −25 °C, to give 0.116 g (25%) of product. Anal. Calcd for $C_{28}H_{20}F_{24}N_8O_2U$: C, 28.15; H, 1.69; N, 9.38. Found: C, 27.85; H, 1.70; N, 8.99.

Acknowledgment. This research was funded by NSF Grant CHE-0617063. We thank the University of California President's Postdoctoral Fellowship Program for partial support of B.M.B. and Dr. Frederick Hollander and Dr. Allen Oliver for expert advice on the crystal structure determinations.

Supporting Information Available: Crystallographic files (CIF), details concerning the crystal structure determinations, and plots showing additional magnetic data. This material is available free of charge via the Internet at http://pubs.acs.org.

IC801303W

(40) *SAINT Software Users Guide*, version 7.0; Bruker Analytical X-ray Systems, Inc.: Madison, WI, 1999.
(41) Sheldrick, G. M. *SADABS*, version 2.03; Bruker Analytical X-ray Systems, Inc.: Madison, WI, 2000.
(42) Sheldrick, G. M. *SHELXTL*, version 6.12; Bruker Analytical X-ray Systems, Inc.: Madison, WI, 1999.
(43) *International Tables for X-ray Crystallography*; Kluwer Academic Pubishers: Dordrecht The Netherlands, 1992; Vol. *C*.